Structural deformation of the $S = 1$ kagome-lattice compound $KV_3Ge_2O_9$

Eigo Takagi,[1] Takuya Aoyama,[1,*] Shigeo Hara,[2] Hirohiko Sato,[3] Tsuyoshi Kimura,[1] and Yusuke Wakabayashi[1,†]
[1]*Division of Materials Physics, Graduate School of Engineering Science, Osaka University, Toyonaka 560-8531, Japan*
[2]*Center for Supports to Research and Education Activities, Kobe University, Kobe 657-8501, Japan*
[3]*Department of Physics, The Institute of Science and Engineering, Chuo University, Kasuga, Bunkyo-ku, Tokyo 112-8551, Japan*
(Received 13 January 2017; published 15 March 2017)

The dielectric and structural properties of the $S = 1$ kagome antiferromagnet $KV_3Ge_2O_9$ are examined. The low-temperature structure below 50 K is orthorhombic with a typical correlation length of 8 nm. While the high-temperature hexagonal phase can be considered C-centered orthorhombic, the C-centered symmetry is broken below 50 K. The low-temperature symmetry does not support the simplex solid state, which is the theoretically expected ground state for the $S = 1$ kagome lattice. Above 60 K, incommensurate lattice modulation is observed. The lock-in transition suggests that the origin of the orthorhombic deformation is the development of a short-range magnetic ordering.

DOI: 10.1103/PhysRevB.95.104416

Antiferromagnetic kagome lattices have long been studied because of the frustrated nature of their magnetism. In $S = 1/2$ cases, where the quantum effect is maximal, the ground state is an exotic quantum spin-liquid state, whose nature is still under debate [1–4]. In the case of $S = 1$ frustrated magnets, the situation can be very different. Spin liquids or spin nematic states have been discussed for $S = 1$ triangular lattices [5–7]. As for theoretical studies of $S = 1$ kagome lattices having nearest-neighbor interactions, the simplex solid state, which is schematically presented in Fig. 1(b), has been suggested by various groups to be the ground state [8–11]. In this state, the upward-pointing triangles and downward-pointing triangles are not equivalent in order to form singlet units by trimerization. The inversion symmetry is spontaneously broken. Taking the biquadratic term $J_{bq} \sum_{\langle ij \rangle} (\boldsymbol{S}_i \cdot \boldsymbol{S}_j)^2$, where $\langle ij \rangle$ denotes nearest-neighbor pairs, into the Hamiltonian, the ground state can be altered. While the ground state remains unchanged for small positive J_{bq}, it turns into a ferroquadrupolar phase [12] when J_{bq} is negative [8,9]. The effect of the next-nearest-neighbor interaction J'' is reported in Ref. [11]. In accordance with other theoretical works, a weak J'' yielded the simplex solid ground state. Both positive and negative J'' stabilize antiferromagnetic ordering, although the magnetic structures are different from each other.

Experimentally, only a few $S = 1$ kagome antiferromagnets, such as NaV_6O_{11} [13,14], m-MPYNN $\cdot$ BF_4 [15,16], and $KV_3Ge_2O_9$ [17], have been reported. Although they appear to be described by the same Hamiltonian, their low-temperature structures and therefore their ground states are different. The magnetic state of the $S = 1$ kagome lattice in NaV_6O_{11} is a singlet state [13] accompanied by an apparent lattice distortion that produces V trimers, keeping the size of the unit cell constant [14]. m-MPYNN $\cdot$ BF_4 is regarded as a $S = 1$ kagome lattice below 20 K [15], and its magnetic ground state is nonmagnetic [18]. Unfortunately, this compound is known to have a structural deformation characterized by the wave vector (1/3, 1/3, 0) below 129 K[16], which is far above the characteristic temperature of magnetism.

$KV_3Ge_2O_9$ appears to be an ideal $S = 1$ kagome lattice. It has no clear magnetic phase transition down to 2 K, and only a bump in magnetic susceptibility around 70 K has been reported [17]. Because its Weiss temperature is -250 K, its magnetism is strongly frustrated. The magnetic ground state of $KV_3Ge_2O_9$ does not seem to be either a singlet state or an antiferromagnetic ordered state [17]. In this paper, we report on the structural properties of the $S = 1$ kagome antiferromagnet $KV_3Ge_2O_9$. Dielectric measurements suggested no signature of the breaking of inversion symmetry. X-ray diffraction measurements showed broad superlattice reflections at low temperatures, indicating that the symmetry changes from hexagonal to orthorhombic below 50 K. The magnetic ground state is discussed based on the low-temperature structure of the compound.

Single crystals of $KV_3Ge_2O_9$ were grown by the hydrothermal method. The outer shape of the crystals was that of a bulky hexagonal column, with a typical volume of 3 mm^3. The space group of the crystals was $P6_3/mmc$, with a- and c-lattice parameters of 5.862 and 13.709 Å, respectively [17]. Throughout this paper, the hexagonal unit cell presented in Fig. 1(a) is generally used; a subscript O is added when the orthorhombic notation is used. Because the simplex solid state breaks the inversion symmetry, we examined the dielectric properties of the single crystals. The real (ε') and imaginary (ε'') parts of the dielectric constant along the a and c axes were measured using an LCR meter (Agilent E4980A) in a frequency (f) range of 0.1 to 200 kHz.

Figure 2(a) shows the temperature (T) dependences of the relative dielectric constants at 1, 10, and 100 kHz along the a (ε'_a; left) and c (ε'_c; right) axes. No clear frequency-independent anomaly was observed, suggesting that no inversion-symmetry-breaking phase transition occurs down to the lowest temperature examined. ε'_a is three to four times larger than ε'_c, showing that the compound is dielectrically active within the c plane. The strong frequency dependences of ε'_a observed in the temperature range 30 to 80 K means that a noticeable dielectric relaxation occurs in this temperature range. This relaxation behavior also appears in the temperature dependence of ε'' along the a axis (ε''_a) as shown in Fig. 2(b).

*Present address: Department of Physics, Graduate School of Science, Tohoku University, Sendai, Miyagi 980-8578, Japan.
†wakabayashi@mp.es.osaka-u.ac.jp

 ©2017 American Physical Society

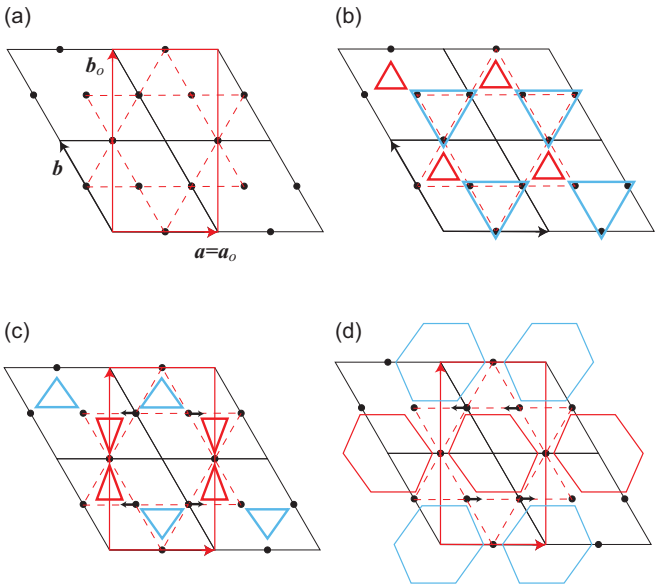

FIG. 1. (a) Hexagonal unit cell ($\boldsymbol{a}$ and $\boldsymbol{b}$) and orthorhombic unit cell ($\boldsymbol{a}_O$ and $\boldsymbol{b}_O$) of a kagome lattice. The cell volume of the orthorhombic cell is twice that of the hexagonal cell; the orthorhombic cell has a C-face-centered symmetry, while the hexagonal cell is primitive. (b) Schematic of the simplex solid state, which is compatible with the original hexagonal unit cell. (c, d) Lattice distortion modes along the $\boldsymbol{a}_O$ direction that are described by the orthorhombic cell.

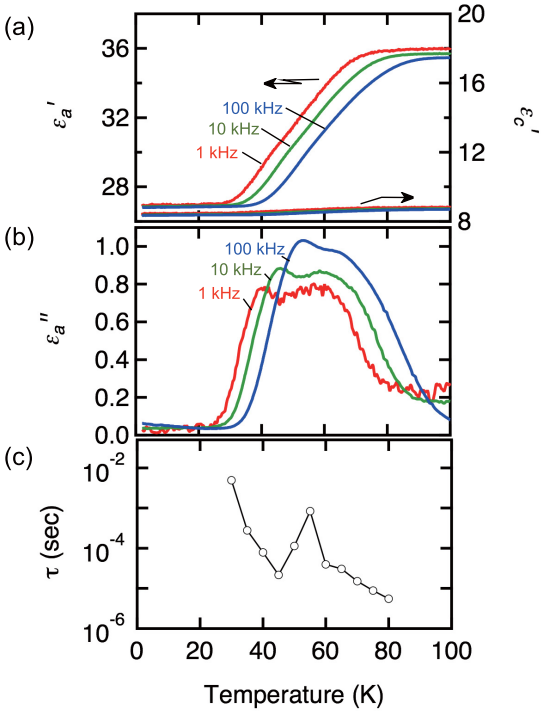

FIG. 2. Temperature profiles of (a) the real and (b) the imaginary parts of the dielectric constant of $KV_3Ge_2O_9$ collected at several frequencies. The left and right vertical axes in (a) indicate the values parallel to the a and c axes, respectively. (c) Temperature variation of the relaxation time.

The double-peak feature indicates that there are two modes of relaxation. The dielectric relaxation time (τ) was examined to study this two-component relaxation. τ was derived from the frequency dependence of isothermal ε_a' by fitting with the empirical Cole-Cole function as reported previously for several relaxor and dispersive dielectrics [19,20]. The temperature dependence of τ is shown in Fig. 2(c). A two-component relaxation behavior is also observed for τ. The gradient of τ, which indicates the excitation energy, drastically changes around 60 K.

Because a broad peak feature in the magnetic susceptibility around 60 K has been reported [17], it was expected that the dielectric relaxation affects (or is induced by) the magnetism through a magnetoelectric or -elastic coupling. However, the effect of the magnetic field on the dielectric constant was less than 0.05% under a magnetic field of 7 T. To investigate the origin of the dielectric and magnetic anomalies observed around 60 K, a structural study was performed.

Single-crystal x-ray diffraction measurements were performed with a four-circle diffractometer attached to an 18-kW Mo rotating anode x-ray source. Incident x rays were monochromatized with a bent graphite crystal. The signal was detected with a CdTe solid-state detector. The typical exposure time for superlattice reflections was 100 s per data point. The sample temperature was controlled with a closed-cycle refrigerator. Some of the measurements were carried out with 11-keV synchrotron x rays at BL-3A of the Photon Factory, KEK, Japan.

The temperature dependences of the lattice parameters are presented in Fig. 3. As shown, the thermal expansion is anisotropic, and the anisotropy is enhanced below 70 K. The width of the rocking curve of the 220 Bragg reflection as a function of the temperature is shown in the inset in Fig. 3. The peak width increased slightly below 100 K, which suggests that the crystal family changes from hexagonal at low temperatures.

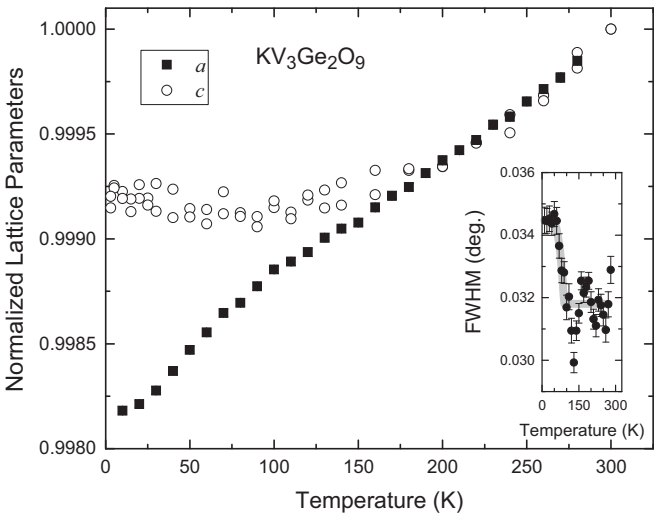

FIG. 3. Temperature variation of the lattice parameters normalized by those measured at 300 K. The a-lattice parameter was measured with synchrotron radiation, while the c-lattice parameter was measured with a laboratory source. Inset: Temperature variation of the 220 rocking curve width. The gray curve is a guide for the eye.

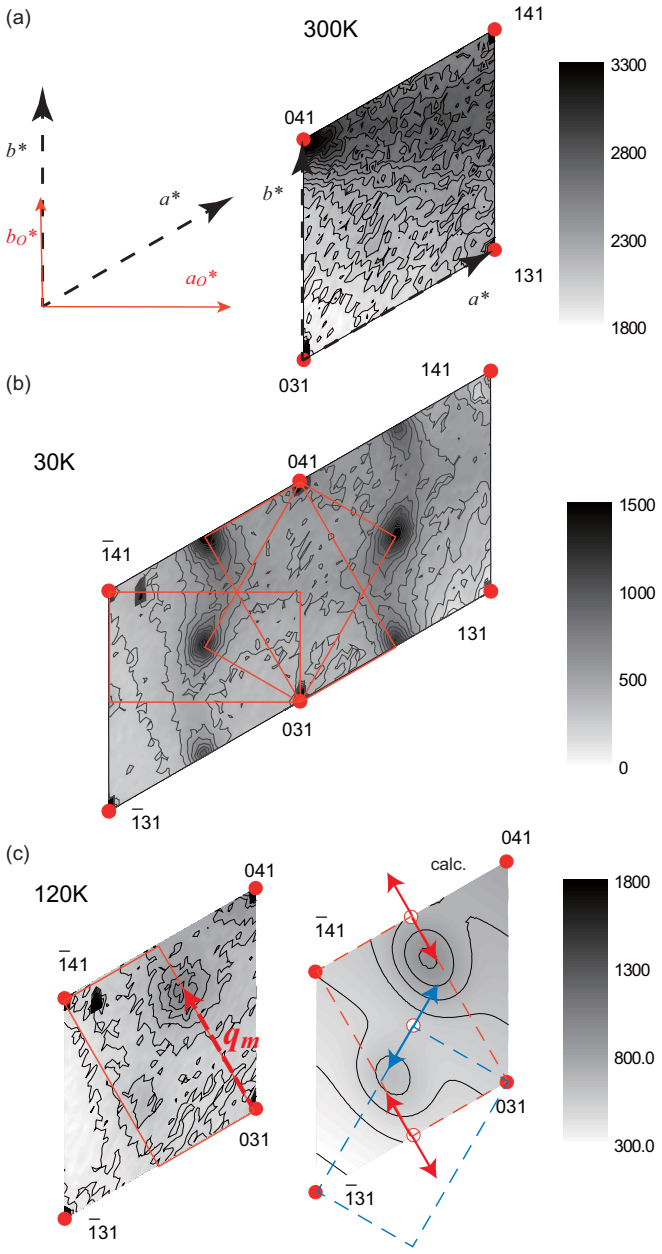

FIG. 4. Scattered intensity distribution around 031 Bragg reflection measured at (a) 300 K, (b) 30 K, and (c) 120 K. Superlattice reflections indexable by multidomain orthorhombic cells are clearly shown at 30 K. At 120 K, the superlattice peaks shift and broaden. The dashed arrow shows the modulation vector $\boldsymbol{q}_m$. The right panel in (c) shows two-dimensional Gaussian fitting results. Open circles show the positions of the superlattice reflections at 30 K. Red and blue arrows indicate the amount of peak splitting.

To clarify the low-temperature structure, we searched for superlattice reflections at 30 K. Scattered x-ray intensity distributions around the 031 Bragg reflection measured at 300 and 30 K are presented in Figs. 4(a) and 4(b). Clear superlattice reflections characterized by the wave vector (1/2, 0,0) (and symmetrically equivalent wave vectors) were observed. The typical peak height was 10^{-4} times as strong as that of typical Bragg reflections. The superlattice peaks were observed only at odd-l positions, indicating that the stacking of the superstructure is antiphase. The peak widths of the superlattice reflections were broad, and the in-plane correlation length was found to be 8 nm. Possible low-temperature unit cells are hexagonal $2\boldsymbol{a} \times 2\boldsymbol{b} \times \boldsymbol{c}$ and orthorhombic $(\boldsymbol{a} + \boldsymbol{b}) \times (\boldsymbol{a} - \boldsymbol{b}) \times \boldsymbol{c} = \boldsymbol{a}_O \times \boldsymbol{b}_O \times \boldsymbol{c}$; corresponding reciprocal lattice vectors for the latter as well as that for the high-temperature hexagonal lattice are shown in Fig. 4(a). Because only the orthorhombic cell accounts for the broadening of the rocking curve presented in the inset in Fig. 3, the orthorhombic structure is found to be the ground state of this compound. In the orthorhombic notation, the high-temperature hexagonal phase is C-centered orthorhombic. The appearance of the superlattice reflections indicates that the C-centered symmetry is broken.

There was no superlattice intensity on the $(0\eta 1)$ line. For example, the (0 3.5 1) position can be indexed as the $(071)_O$ reciprocal lattice point in the orthorhombic cell, which has no intensity as shown in Fig. 4(b). This result means that the atomic displacement is parallel to the $\boldsymbol{a}_O$ direction, because the superlattice intensity is proportional to $|\boldsymbol{Q} \cdot \boldsymbol{u}|^2$, where $\boldsymbol{Q}$ and $\boldsymbol{u}$ denote the scattering vector and the displacement, respectively [21].

The lack of C-centered symmetry induced by the lattice distortion along the $\boldsymbol{a}_O$ direction leads us to the structural models presented in Figs. 1(c) and 1(d), which are both centrosymmetric. The structure presented in Fig. 1(c) has the same symmetry with resonating bow ties as that suggested in Ref. [22]. The distortion mode [Fig. 1(c)] causes some intensity at $(hk1)_O$ with h:even and k:odd but does not cause any intensity at h:odd and k:even. The mode in Fig. 1(d) has reversed superlattice reflection conditions. The experimental results show no distinct reflection conditions in the $l = 1$ plane except for the absence of $h_O = 0$ peaks, indicating that both modes are involved in the real low-temperature structure.

The superlattice peaks shift their positions with increasing temperature. Figures 4(b) and 4(c) show the maps obtained at 30 and 120 K. The superlattice peaks at 30 K are at commensurate positions, while those at 120 K are at incommensurate positions. The temperature variations of the superlattice peak intensity, position, and peak width obtained from the line profiles along the $(\delta, 3 + \delta, 1)$ line are summarized in Fig. 5. The peak intensity decreases monotonically with increasing temperature. Although we could not see any superlattice reflection above 280 K, a clear phase transition temperature was barely observed in the temperature variation of the integrated intensity. In contrast, a distinct lock-in transition is clearly shown at 55 ± 5 K in Fig. 5(b). The peak width observed for the incommensurate phase is broader than that for the commensurate phase; the correlation length above 100 K is 5 nm.

The incommensurate peak positions can be indexed by the multidomain structure of the uniaxially incommensurate orthorhombic lattice. Two-dimensional multi-Gaussian fitting [23] of Fig. 4(c) gave the modulation vector $\boldsymbol{q}_m$ at 120 K as $0.73\boldsymbol{a}_O^*$, or $0.36(\boldsymbol{a}^* + \boldsymbol{b}^*)$ in the hexagonal setting used in Fig. 5(b). The intensity distribution in the wide region of the reciprocal space was consistent with the atomic displacement parallel to the $\boldsymbol{a}_O$ direction, i.e., a longitudinal modulation.

Let us examine the magnetic ground state of this compound based on our structural observations. The ground state of the

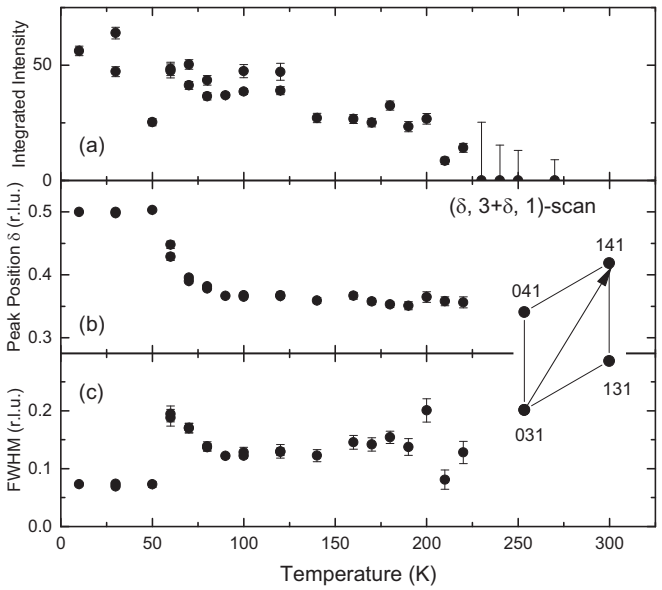

FIG. 5. Temperature variation of the superlattice reflection on the $(\delta\ 3+\delta\ 1)$ line. (a) Integrated intensity, (b) peak position, and (c) peak width are presented.

$S = 1$ kagome lattice with nearest-neighbor antiferromagnetic interaction is reported to be the simplex solid state [8–11], which is depicted in Fig. 1(b). However, the low-temperature structure and the reported magnetism [17] cannot be explained by the simplex solid state. This result leads us to take other terms in the Hamiltonian into account. One possible origin of the orthorhombic symmetry may be the ferroquadrupolar state [12]. According to Ref. [9], this state is stabilized by a slight amount (12% of the bilinear term) of the negative biquadratic term. Although it is ambiguous that the ferroquadrupolar state can cause a noticeable amount of lattice deformation, it is likely to have some amount of lattice deformation through the spin-orbit coupling because octahedrally coordinated V ions with two t_{2g} electrons can have orbital angular momentum. The low-temperature orthorhombic symmetry is consistent with the ferroquadrupolar state, while it is unclear how the incommensurate structure is developed from the ferroquadrupolar state. In terms of macroscopic magnetic properties, the nematic state does not differ from that of antiferromagnets [12], and therefore the confirmation of this state is challenging. Another possibility is the development of antiferromagnetic order. Because the exchange interaction is related to the crystal structure, atomic displacement can alter the magnetic structure, or vice versa. If the lattice distortion presented in Fig. 1(c) occurs, the periodicity of the exchange interaction along the a_O direction is doubled. In the case of the distortion shown in Fig. 1(d), the triangles are no longer regular ones but nonequilateral ones. These distortions lift the frustration, and magnetic order can develop. Even in this case, the correlation length of the magnetic ordering must be short, because the experimentally observed correlation length of the lattice distortion is short. The incommensurate structure above 60 K supports the development of the short-range magnetic ordering. It is well known that first- and second-neighbor exchange interactions stabilizing different magnetic structures can cause an incommensurate magnetic ordering at certain temperatures [24–26].

The dielectric properties show two distinct features: first, the dielectric constant along the c axis is much smaller than the in-plane one, and second, the dielectric relaxation time shows a sudden change at 60 K. The former feature implies that the atomic displacement in this compound has a high in-plane amplitude. Because the superlattice reflections originate from the atomic displacement along the a_O direction, this displacement should be related to the dielectric property. The latter feature is, therefore, caused by the lock-in transition. The restoring force is suppressed at the transition temperature, which causes the slow relaxation time.

To summarize, a low-temperature structural study of $KV_3Ge_2O_9$ has been performed for the first time. The $S = 1$ kagome lattice has a slight amount of orthorhombic lattice deformation that breaks its C-centered symmetry. The correlation length of the orthorhombic domain is ~8 nm. The atomic displacement from the high-temperature hexagonal structure is along the a_O direction. There is a lock-in transition at 55 ± 5 K, and the incommensurate wave vector above 100 K is $0.73\boldsymbol{a}^*_O$. The superlattice reflection disappears above 280 K. The lock-in transition exhibits some relation to the dielectric relaxation time. The magnetic state of the V ions in the orthorhombic phase is discussed and is likely to be a short-range magnetic ordered phase.

This work was supported by a Grant-in-Aid for Scientific Research (JSPS KAKENHI Grant No. JP26105008). The synchrotron radiation experiments at the Photon Factory were performed with the approval of the Photon Factory Program Advisory Committee (Proposal Nos. 2012G091 and 2014S2-003).

[1] S. Yan, D. A. Huse, and S. R. White, Spin-liquid ground state of the $S = 1/2$ kagome Heisenberg antiferromagnet, Science **332**, 1173 (2011).

[2] S. Depenbrock, I. P. McCulloch, and U. Schollwöck, Nature of the Spin-Liquid Ground State of the $S = 1/2$ Heisenberg Model on the Kagome Lattice, Phys. Rev. Lett. **109**, 067201 (2012).

[3] H.-C. Jiang, Z. Wang, and L. Balents, Identifying topological order by entanglement entropy, Nat. Phys. **8**, 902 (2012).

[4] Y. Iqbal, D. Poilblanc, and F. Becca, Spin-$\frac{1}{2}$ Heisenberg J_1-J_2 antiferromagnet on the kagome lattice, Phys. Rev. B **91**, 020402 (2015).

[5] S. Nakatsuji, Y. Nambu, H. Tonomura, O. Sakai, S. Jonas, C. Broholm, H. Tsunetsugu, Y. Qiu, and Y. Maeno, Spin disorder on a triangular lattice, Science **309**, 1697 (2005).

[6] H. Tsunetsugu and M. Arikawa, Spin nematic phase in $S = 1$ triangular antiferromagnets, J. Phys. Soc. Jpn. **75**, 083701 (2006).

[7] S. Bhattacharjee, V. B. Shenoy, and T. Senthil, Possible ferro-spin nematic order in $NiGa_2S_4$, Phys. Rev. B **74**, 092406 (2006).

[8] H. J. Changlani and A. M. Läuchli, Trimerized ground state of the spin-1 Heisenberg antiferromagnet on the kagome lattice, Phys. Rev. B **91**, 100407 (2015).

[9] T. Liu, W. Li, A. Weichselbaum, J. von Delft, and G. Su, Simplex valence-bond crystal in the spin-1 kagome Heisenberg antiferromagnet, Phys. Rev. B **91**, 060403 (2015).

[10] S. Nishimoto and M. Nakamura, Non-symmetry-breaking ground state of the $S = 1$ Heisenberg model on the kagome lattice, Phys. Rev. B **92**, 140412 (2015).

[11] P. Ghosh, A. K. Verma, and B. Kumar, Plaquette-triplon analysis of magnetic disorder and order in a trimerized spin-1 kagome Heisenberg antiferromagnet, Phys. Rev. B **93**, 014427 (2016).

[12] K. Penc and A. M. Läuchli, Spin nematic phases in quantum spin systems, in *Introduction to Frustrated Magnetism: Materials, Experiments, Theory*, edited by C. Lacroix, P. Mendels, and F. Mila (Springer, Berlin, 2011), p. 331.

[13] H. Kato, M. Kato, K. Yoshimura, and K. Kosuge, ^{23}Na-NMR study in NaV_6O_{11}, J. Phys. Soc. Jpn. **70**, 1404 (2001).

[14] Y. Kanke, F. Izumi, Y. Morii, E. Akiba, S. Funahashi, K. Kato, M. Isobe, E. Takayama-Muromachi, and Y. Uchida, Structural phase transitions in the ferromagnetic vanadium oxide NaV_6O_{11}, J. Solid State Chem. **112**, 429 (1994).

[15] K. Awaga, T. Okuno, A. Yamaguchi, M. Hasegawa, T. Inabe, Y. Maruyama, and N. Wada, Variable magnetic interactions in an organic radical system of (*m-N*-methylpyridinium α-nitronyl nitroxide)X^-: A possible kagome antiferromagnet, Phys. Rev. B **49**, 3975 (1994).

[16] T. Kambe, Y. Nogami, K. Oshima, W. Fujita, and K. Awaga, Structural phase transition in two-dimensional kagome antiferromagnet m-N-methylpyridinium α-nitronyl nitroxide $\cdot BF_4 \cdot$ 1/3 (acetone), J. Phys. Soc. Jpn. **73**, 796 (2004).

[17] S. Hara, H. Sato, and Y. Narumi, Exotic magnetism of novel $S = 1$ kagome lattice antiferromagnet $KV_3Ge_2O_9$, J. Phys. Soc. Jpn. **81**, 073707 (2012).

[18] N. Wada, T. Kobayashi, H. Yano, T. Okuno, A. Yamaguchi, and K. Awaga, Observation of spin-gap state in two-dimensional spin-1 Kagome antiferromagnet *m*-MPYNN $\cdot BF_4$, J. Phys. Soc. Jpn. **66**, 961 (1997).

[19] A. A. Bokov, M. A. Leshchenko, M. A. Malitskaya, and I. P. Raevski, Dielectric spectra and Vogel-Fulcher scaling in $Pb(In_{0.5}Nb_{0.5})O_3$ relaxor ferroelectric, J. Phys.: Condens. Matter **11**, 4899 (1999).

[20] F. Schrettle, P. Lunkenheimer, J. Hemberger, V. Yu. Ivanov, A. A. Mukhin, A. M. Balbashov, and A. Loidl, Relaxations as Key to the Magnetocapacitive Effects in the Perovskite Manganites, Phys. Rev. Lett. **102**, 207208 (2009).

[21] A. Guinier, *X-ray Diffraction in Crystals, Imperfect Crystals, and Amorphous Bodies* (Dover, Mineola, NY, 1994), Section 7.2.1.

[22] S. V. Isakov and Y. Baek Kim, Quantum order by disorder in a spin-one frustrated magnet on the kagome lattice, Phys. Rev. B **79**, 094408 (2009).

[23] Two-dimensional multi-Gaussian fitting was performed with the assumption that the superlattice reflections observed at 30 K are split along the $\boldsymbol{a}_O^*$ direction [red and blue arrows in Fig. 4(c)]. The intensity of each split peak was assumed to be proportional to the peak intensity at 30 K.

[24] P. Bak and J. von Boehm, Ising model with solitons, phasons, and "the devil's staircase," Phys. Rev. B **21**, 5297 (1980).

[25] S. L. Qiu, M. Dutta, H. Z. Cummins, J. P. Wicksted, and S. M. Shapiro, Extension of the Lifshitz-point concept to first-order phase transitions: Incommensurate $NaNO_2$ in a transverse electric field, Phys. Rev. B **34**, 7901 (1986).

[26] T. Kimura, S. Ishihara, H. Shintani, T. Arima, K. T. Takahashi, K. Ishizaka, and Y. Tokura, Distorted perovskite with e_g^1 configuration as a frustrated spin system, Phys. Rev. B **68**, 060403 (2003).